DYNAMICS OF THE QUIET UPPER SOLAR ATMOSPHERE IN THE NETWORK

Peter Gömöry[(1)], Ján Rybák[(1)], Aleš Kučera[(1)], Werner Curdt[(2)], and Hubertus Wöhl[(3)]

[(1)]Astronomical Institute, SAS, 05960 Tatranská Lomnica, Slovakia
[(2)]Max-Planck-Institute für Sonnensystemforschung, 37191 Katlenburg-Lindau, Germany
[(3)]Kiepenheuer-Institut für Sonnenphysik, 79104 Freiburg, Germany

ABSTRACT

The temporal evolution of the spectral parameters of the chromospheric He I 584.33 Å and the transition region O V 629.73 Å emission lines measured by the Coronal Diagnostic Spectrometer (CDS) in/above the supergranular network near disk center was constructed in order to examine the correlation of the spectral line intensities and the Doppler shifts. The arithmetic process of the correct calculation of the cross-correlation function is shown here in details. The necessity of edge data removal and the subtraction of any background trends before applying the cross-correlation function was revealed. The method was verified using the test example of two ideal sinusoidal functions. Resulting cross-correlation functions were analyzed with a view to describe energy transfer and mass motion between chromosphere and transition region in the particular network. The maximum value ($CC_{max} = 0.46$) of the cross-correlation function of the He I and the O V line intensities was achieved for a time lag of +27.3 s, i.e. some changes in the O V line intensities precede changes in the He I line intensities. In contrast, the cross-correlation function of the Doppler shifts of these lines reached the maximum value ($CC_{max} = 0.53$) for a time lag of 0 seconds. In summary, we can assume that the non-radiative energy was transported from the transition region down to the chromosphere without any significant mass motion in the studied network element.

1. INTRODUCTION

First measurements of the solar emission in the UV and EUV part of the electromagnetic spectra taken by Skylab, Solar Maximum Mission and NRL High Resolution Telescope and Spectrograph revealed that the upper solar atmosphere, from chromosphere to corona, is not static but in the contrary, a very dynamic and inhomogeneous environment (Mariska, 1992). In a view of the new results the chromospheric plasma was separated into two regions: magnetic network and non-magnetic intranetwork; small-scale eruptive events were discovered in the transition region. These results were later confirmed using instruments onboard of the Solar and Heliospheric Observatory (SOHO) (Domingo et al., 1995). But the answer to the question how the energy is transfered into the upper solar atmosphere is still open. For identification of possible mechanisms it is necessary to observe all parts of the upper solar atmosphere simultaneously. This requirement can be fulfilled using the Coronal Diagnostic Spectrometer (CDS) (Harrison et al., 1995) which is able to detect simultaneously spectral lines formed in a wide temperature interval. The analysis of the cross-correlation between the chromospheric and the transition region spectral line intensities and the Doppler shifts should allow us to study the mutual connections between these atmospheric layers, e.g. energy transfer and mass motion. This method was already used for the diagnostics of the chromospheric dynamics when Bocchialini and Baudin (1995) studied the cross-correlation function of the Doppler shifts of two chromospheric spectral lines (He I 10830 Å, Ca II K 3934 Å) and suggested the presence of downward propagating waves in the network. On the other hand cross-correlations are also used in stellar astronomy for overlapping spectra (Zverko et al., 1994). The correct algorithm to calculate the cross-correlation functions as well as the results obtained for the chromospheric (He I) and the transition region (O V) spectral lines are presented in this contribution.

2. DATA

The dataset, analyzed in this contribution, was obtained by the normal incidence part (NIS) of CDS (Harrison et al., 1995) on 14 May 1998 between 23^h25^m and

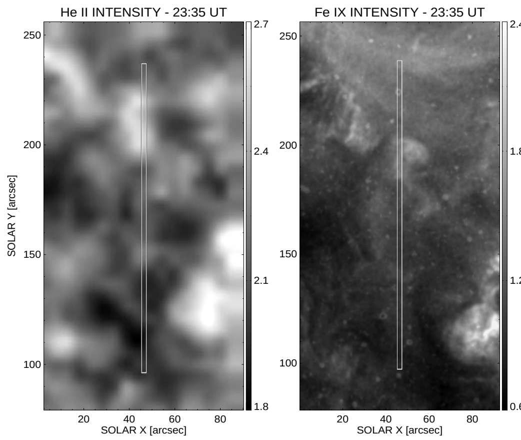

Figure 1. CDS slit position in the context images taken with SOHO/EIT (left) and TRACE (right) instruments in the He II 304 Å (log $T_e = 4.9$) and the Fe IX 171 Å (log $T_e = 6$) spectral channels at the moment which corresponds to the middle of the CDS measurements, respectively. The coordinates of the CDS slit center are: x = 46.4"; y = 167.1". The coordinate system is given relative to the disk center. The intensity values given in $W m^{-2} sr^{-1} Å^{-1}$ and in counts s^{-1} respectively, are displayed in logarithmic scale.

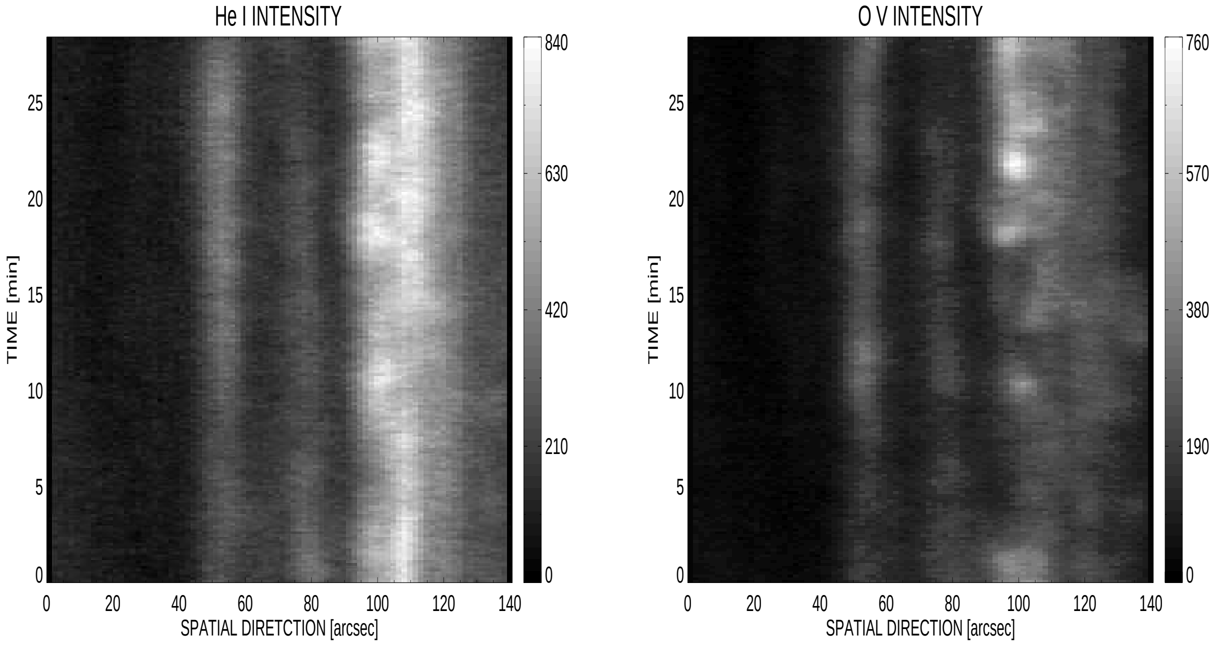

Figure 2. 2D space-time maps of the He I *and the O* V *line intensities. The studied area, so-called typical network, is shown in the area between 111" and 116". The intensity values are given in erg $cm^{-2}s^{-1}sr^{-1}\AA^{-1}$. The horizontal axis describes spatial direction and the vertical axis describes time. The solar rotation was not compensated, so the vertical axis presents the spatial extent of the observed solar features as well.*

23^h53^m as a part of the joint observing program JOP 78.[1] Two bright spectral lines of the NIS spectral range, the chromospheric spectral line He I 584.33 Å (log T = 4.5) and the transition region spectral line O V 629.73 Å (log T = 5.4) (Mazzotta et al., 1998; Young et al., 2003), were chosen for observations in order to study properties of the quiet Sun supergranular network near disk center (Fig. 1). A 1729 s (∼28.8 min) long dataset of 190 spectral images with exposure time 5 s and with a cadence of 9.1 s was obtained. The present data were acquired using the 2" wide slit (oriented in the north – south direction) in sit-and-stare mode, i.e. the pointing was kept fixed and the solar rotation was not compensated. Therefore the slit has rastered an area almost 4.4" wide in the east – west direction during the observations.

3. DATA REDUCTION

Before a detailed analysis the data were corrected for the most obvious instrumental features of the CDS/NIS instrument[2]. The basic photometry reduction was provided using the standard CDS software. The data were then converted from counts into absolute units. Finally, a single Gaussian function F(x)

$$F(x) = A.exp\left[-\frac{1}{2}\left(\frac{x-v}{w}\right)^2\right], \qquad (1)$$

where A is the amplitude (intensity), v is the maximum position and w is the line width, was fitted to each spectral profile. This was accomplished using the standard routine CFIT[3] which is based on the Levenberg-Marquardt method of minimalization of the least squares (Press et al., 1986). The line intensities and the Doppler shifts were then estimated as our primary data. Used fitting procedure also allowed to determine the square root errors of the primary data. The wavelength scales were adjusted using the overall redshift of the transition region spectral lines (Peter & Judge, 1999), which was found to be ∼10 km/s for the O V spectral line, and the laboratory wavelengths of the He I and the O V lines (Macpherson & Jordan, 1999). The resulting 2D space-time maps of the He I and the O V line intensities are displayed on Fig. 2. Only primary data which were estimated with a fit uncertainity χ^2 lower than 10 erg^{2}cm^{-4}s^{-2}sr^{-2}Å^{-2} were used for the following analysis.

4. RESULTS

Only the particular part of the supergranular network (so-called "typical network"), displayed on the Fig. 2 between 111" and 116", was chosen for the analysis. This area was not influenced by the explosive event which was detected in the O V spectral line between 97" – 102" along the slit and in time between 17.7 min – 18.9 min from the beginning of the measurements (Gömöry et al., 2003). The averaged temporal variations of the He I and the O V line intensities (Fig. 3) and the Doppler shifts were created as spatial average over four primary data (∼7") from the selected pixels along the slit in each exposure. The

[1] JOP 78 proposal: www.astro.sk/∼choc/jop078_prop/

[2] Details: http://solg2.bnsc.rl.ac.uk/software/uguide/uguide.shtml

[3] Details: CDS Software Note nr. 47

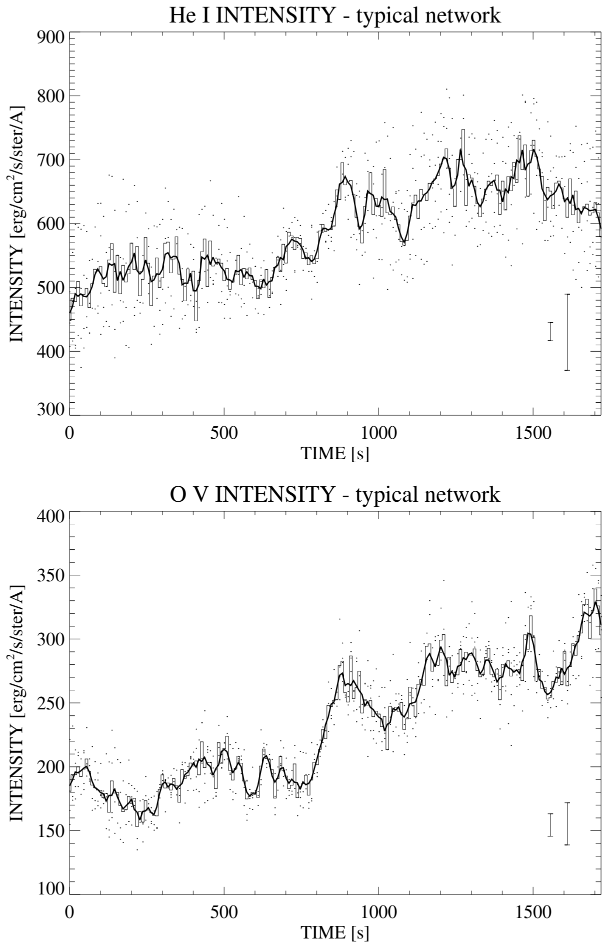

Figure 3. *Temporal variations of the He* I *(top panel) and the O* V *(bottom panel) line intensities in the typical network. The dots show primary data (four values of four pixels along the slit), histograms display the averaged temporal variations of the primary data, and the thick lines show the smoothed variations of the averaged data. The typical square root errors of the primary data (derived from the fitting of the spectral profiles) are* $\pm$ *14.2* $erg\,cm^{-2}s^{-1}sr^{-1}\AA^{-1}$ *for the He* I *line and* $\pm$ *8.8* $erg\,cm^{-2}s^{-1}sr^{-1}\AA^{-1}$ *for the O* V *line (left error bars), respectively. The mean standard deviations of the primary data from the displayed averaged temporal variations are* $\pm$ *59.6* $erg\,cm^{-2}s^{-1}sr^{-1}\AA^{-1}$ *for the He* I *line and* $\pm$ *16.5* $erg\,cm^{-2}s^{-1}sr^{-1}\AA^{-1}$ *for the O* V *line (right error bars), respectively.*

standard deviation of the primary data from the averaged values were also figured out. Each averaged variation was finally smoothed using the running mean of five points (Fig. 3).

The cross-correlation function of the averaged and smoothed temporal variations of the He I and the O V line intensities was calculated in order to study the time shifts between local changes in both variations. The most common method of the calculation of the cross-correlation function ($P_{xy}(L)$) of two sample populations $x = (x_1, x_2, x_3, ..., x_N)$ and $y = (y_1, y_2, y_3, ..., y_N)$ as a function of the time shift L between x and y populations is based on the Pearson's algorithm. In this case the $P_{xy}(L)$ is given by the formula

$$P_{xy}(L) = \frac{\sum_{k=1+L}^{N+L}(x_k - \bar{x}) . \sum_{k=1}^{N}(y_k - \bar{y})}{\sqrt{\sum_{k=1+L}^{N+L}(x_k - \bar{x})^2} . \sqrt{\sum_{k=1}^{N}(y_k - \bar{y})^2}}, \qquad (2)$$

for $L \geq 0$, where $\bar{x}$ and $\bar{y}$ are the means of the sample populations (Press et al., 1986). Since, the number of variables of both sample populations x and y is N, those variables x_k for which the index k was greater than N were generated using the first member of the sample population x, i.e. if the $L = 1$ than $x_{N+1} = x_1$. Similarly the second part of the cross-correlation function ($L < 0$) was calculated using the same formula but the sum boundaries were modified. The cross-correlation function of the He I and the O V line intensities (Fig. 3) calculated using the Pearson's algorithm is shown in Fig. 4 (top panel). As one can see, this cross-correlation function has an asymmetric shape and it reaches high values for time shifts in the interval (-200 s, 0s). This would indicate that the changes happened firstly in the He I line intensities and then in the O V line intensities. However, comparison of the temporal variations of these spectral line intensities (Fig. 3) does not support this prediction. Calculation of the cross-correlation function seems to be affected by a signal which was added to the original temporal variations. This signal was found to be generated by moving of the edge data from the beginning (lower intensities) to the end (higher intensities) of the temporal variations in order to create effect of the time shift between variations according equation (2) and explanation given above. Therefore, the cross-correlation function was calculated again but using only those parts of temporal variations of the spectral line intensities which were not affected while creating the time shifts. Value of the time shift has determined the number of the edge data which were cut off from the temporal variations before calculation of the cross-correlation function, using the following formula

$$P_{xy}^{'}(L) = \frac{\sum_{k=1+L}^{N}(x_k - \bar{x}) . \sum_{k=1}^{N-L}(y_k - \bar{y})}{\sqrt{\sum_{k=1+L}^{N}(x_k - \bar{x})^2} . \sqrt{\sum_{k=1}^{N-L}(y_k - \bar{y})^2}}, \qquad (3)$$

for $L \geq 0$, where the variables have the same meaning as before and the calculation of the cross-correlation coefficients for the negative time shifts L was provided in the same sense as it is described above. Newly calculated cross-correlation function of the He I and the O V line intensities (Fig. 4; middle panel) reaches high values in the whole interval of the time shifts. This could indicate that the shape of the cross-correlation function is still influenced by some general trend in the temporal variations which is present over the whole temporal interval, e.g. a linear increase of the temporal variations of the He I and the O V line intensities which is clearly visible in Fig. 3. Subtraction of the linear trend from the temporal variations before calculation finally led to the correct cross-correlation function (Fig. 4; bottom panel)

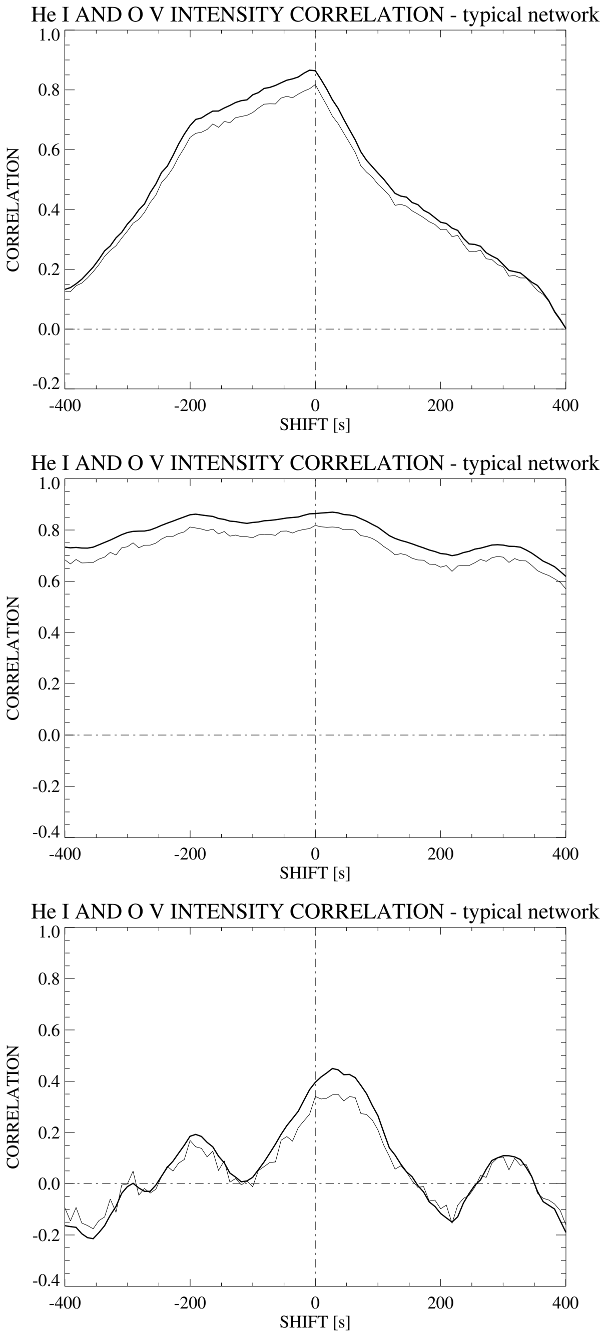

Figure 4. Cross-correlation functions of the He I *and the O* V *line intensities illustrating the arithmetic process used for the correct calculation of the final cross-correlation function. The thin lines show cross-correlation functions of the averaged variations and the thick lines represents cross-correlation functions of the smoothed variations shown also in Fig. 3. Top: The cross-correlation function calculated using Pearson's algorithm given by eq. (2). Middle: The shape of the cross-correlation function calculated when the edge data were not taken into account (eq. 3). Bottom: Final cross-correlation function calculated after subtraction of a linear trend from the temporal variation (eq. 4).*

which was calculated using the following formula

$$P''_{xy}(L) = \frac{\sum_{k=1+L}^{N}(X_k - \bar{X}).\sum_{k=1}^{N-L}(Y_k - \bar{Y})}{\sqrt{\sum_{k=1+L}^{N}(X_k - \bar{X})^2}.\sqrt{\sum_{k=1}^{N-L}(Y_k - \bar{Y})^2}}, \tag{4}$$

for $L \geq 0$, where $X = (X_1, X_2, X_3, ..., X_N)$ and $Y = (Y_1, Y_2, Y_3, ..., Y_N)$ are the same sample populations like before but corrected for the linear trend, and $\bar{X}$ and $\bar{Y}$ are the means of these corrected populations (for the explanation of the calculation of the cross-correlation function for the negative time shifts L see text above). This final cross-correlation function reaches maximum for time shifts symmetrically centered around +27.3 s.

The necessity for subtraction of the linear trend from the temporal variations can be demonstrated also using test data (Fig. 5). Cross-correlation function of two ideal sinusoidal variations with a period of 200 s which are superposed on the linear trend (Fig. 5, top left panel) achieved only positive values in the whole interval of the time shifts (Fig. 5, top right panel). In this case the expected anti-correlations (negative values of the correlation coefficients) for time shifts $= \pm 100$ s and ± 300 s do not appear. The correct shape of the cross-correlation function (Fig. 5, bottom right panel) was obtained only after subtraction of the linear trend from both variations (Fig. 5, bottom left panel).

The temporal variations of the He I and the O V line Doppler shifts were not superposed on any significant general trend. Therefore, the calculation of their final cross-correlation function was directly performed using formula (3). The subtraction of the linear trend from the temporal variations of the spectral line Doppler shifts was tested but no significant changes between cross-correlation functions calculated using the formula (3) and the formula (4) were found. In this case the cross-correlation function reaches the maximum for the time shift equal to 0 s (not shown here).

5. DISCUSSION AND CONCLUSIONS

The studied temporal variations of the He I and the O V line intensities and the Doppler shifts were compared to similar work published by Gallagher et al. (1999). Our analysis confirmed the simultaneous increase of the He I and the O V line intensities in/above supergranular network. But in contrast, different shapes of temporal variations were obtained for the He I and the O V line Doppler shifts.

Our detailed analysis has shown the necessity to avoid the edge data effect and to subtract any general trend (e.g. long-term increase) on which the data are superposed from the temporal variations before calculation of their cross-correlation function. This was demonstrated using the test example where the cross-correlation function of two ideal sinusoidal functions which were superposed on the linear trend never reaches negative values although one should expect it. The correct shape of the

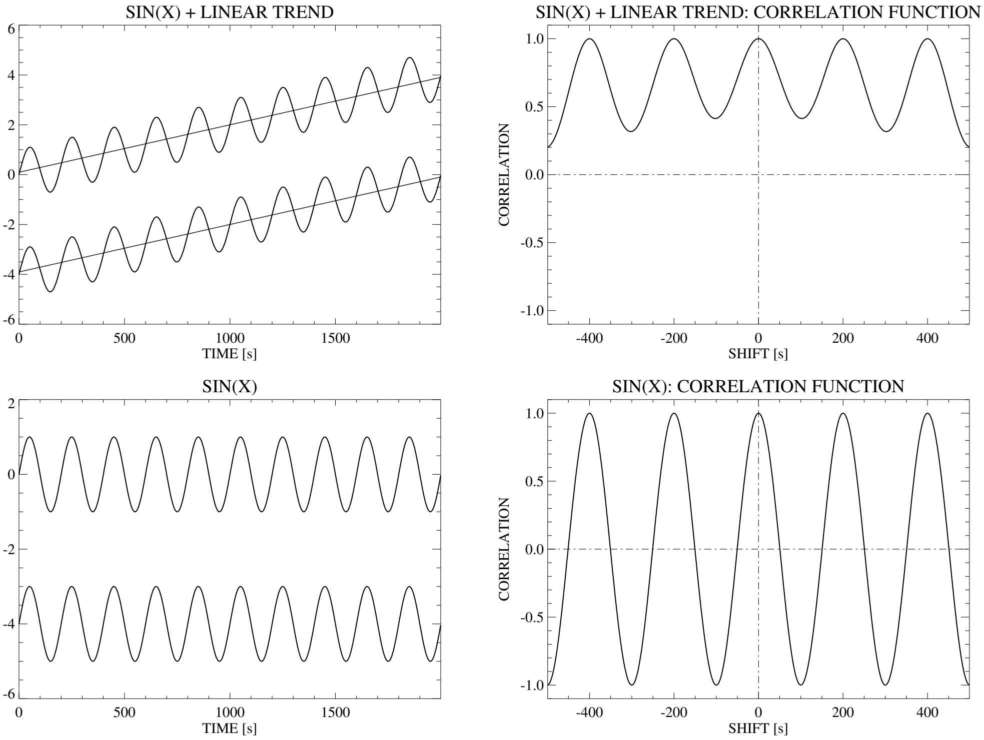

Figure 5. Demonstration of the necessity for linear trend subtraction from compared signals. Top: Two ideal sinusoidal functions with periods of 200 s superposed on a linear trend (left panel) and their cross-correlation function (right panel). This cross-correlation function achieves only positive values which is in contrast with expected anti-correlations of the sinusoidal function for time shifts = $\pm$100 s and $\pm$300 s. Bottom: Sinusoidal functions after subtraction of the linear trend (left panel). In this case their cross-correlation function has obtained the expected shape (right panel).

cross-correlation function was obtained only after subtraction of the general trend from both variations.

Using the described method to calculate the cross-correlation function a value of $+27.3 \pm 4.55$ s resulted for the time shift between temporal variations of the He I and the O V line intensities. It means that some observed changes were achieved firstly in the O V line intensities and then in the He I line intensities. Contrary to this result, the cross-correlation function of the He I and the O V line Doppler shifts reaches a sharp maximum for a time shift of 0 ± 4.55 s, i.e. the macroscopic motion of the chromospheric and transition region plasma happened simultaneously. Following these results we can assume that the non-radiative energy was transferred from the transition region to the chromosphere without any significant mass motion in the particular network under study.

ACKNOWLEDGMENTS

SOHO is a project of international cooperation between ESA and NASA. P.G., J.R. and A.K. are grateful to the Slovak grant agency VEGA for supporting of this work (grant No. 2/3015/23). This research is part of the European Solar Magnetism Network (EC/RTN contract HPRN-CT-2002-00313).

REFERENCES

Bocchialini, K., Baudin, F.: 1995, *Astron. Astrophys.* **299**, 893

Domingo, V., Fleck, B., Poland, A.I.: 1995, *Solar Phys.* **162**, 1

Gallagher, P.T., Phillips, K.J.H., Harra-Murnion, L.K., Baudin, F., Keenan, F.P.: 1999, *Astron. Astrophys.* **348**, 251

Gömöry, P., Rybák, J., Kučera, A., Curdt, W., Wöhl, H.: 2003, *Hvar Obs. Bull.* **27**, 67

Harrison, R.A., Sawyer, E.C., Carter, M.K., et al.: 1995, *Solar Phys.* **162**, 233

Macpherson, K.P., Jordan, C.: 1999, *MNRAS* **308**, 510

Mariska, J.T.: 1992, *The Solar Transition Region*, Cambridge University Press, Cambridge

Mazzotta, P., Mazzitelli, G., Colafrancesco, S., Vittorio, N.: 1998, *Astron. Astrophys. Suppl.* **133**, 403

Peter, H., Judge, P.G.: 1999, *Astrophys. Journal* **522**, 1148

Press, W.H., Flanery, B.P., Teukolsky, S.A., Vetterling, W.T.: 1986, *Numerical Recipes*, Cambridge University Press, Cambridge

Young, P.R., Del Zanna, G., Landi, E., et al.: 2003, *Astrophys. Journal Suppl.* **144**, 135

Zverko, J., Zboril, M., Žižňovský, J.: 1994, *Astron. Astrophys.* **283**, 932